A Parameterization for the Absorption of Solar Radiation in the Earth's Atmosphere

Andrew A. Lacis

Computer Sciences Corporation, New York, N. Y. 10025

James E. Hansen

Goddard Institute for Space Studies, New York, N. Y. 10025

(Manuscript received 10 August 1973, in revised form 9 October 1973)

ABSTRACT

A method is described for rapidly computing the amount of solar energy absorbed at the earth's surface and in the atmosphere as a function of altitude. The method is a parametric treatment, but the form of the solution and the coefficients involved are based on accurate multiple-scattering computations. In this treatment the absorption varies with the amount and type of clouds, the humidity, the zenith angle of the sun, and the albedo of the earth's surface. Within the stratosphere the absorption also depends on the vertical distribution of ozone.

This parameterization for solar radiation is being used in current versions of the global atmospheric circulation model developed at the Goddard Institute for Space Studies.

1. Introduction

Solar radiation absorbed at the earth's surface and in the atmosphere is the initial source of energy causing atmospheric motions. A reliable treatment of solar radiation in numerical models of the atmospheric circulation is required for long-range weather forecasts and for climatological studies.

In computations of absorption it is important that the radiatively significant constituents of the atmosphere be treated as variables. This allows the circulation model to be used for investigating the effects of possible changes in the atmospheric composition, including "feedbacks" through the atmospheric dynamics which may magnify or diminish the initial effect of the changes.

The major difficulty in computing the absorption of solar radiation is in correctly incorporating the effects of multiple scattering. As Goody (1964, Chap. 6) points out, scattered solar radiation is usually neglected "for reasons which are rarely stated explicitly, but which may well represent a desire to avoid a particularly difficult problem." Although many "exact" methods are available for solving the monochromatic equation of transfer, they are not appropriate for numerical circulation models because 1) the frequency integration over the solar spectrum would result in a computational burden exceeding that for the modeling of the atmospheric circulation, and 2) only approximate values can be supplied for atmospheric optical proper-

ties,[1] thus nullifying any potential gain in numerical precision. What is needed is an approximate treatment which reliably models the effects of multiple scattering, takes negligible computer time, and yields an accuracy consistent with the knowledge of atmospheric composition and optical properties.

The principal absorbers in the earth's atmosphere are water vapor in the troposphere and ozone in the stratosphere. Water vapor absorbs primarily in the near-infrared region, $0.7~\mu m \lesssim \lambda \lesssim 4~\mu m$. At shorter wavelengths the main gaseous absorber is ozone (O_3), which is effective in the ultraviolet ($\lambda \lesssim 0.35~\mu m$) and in the visual ($0.5~\mu m \lesssim \lambda \lesssim 0.7~\mu m$). Fig. 1, taken from Pettit (1951), is representative of the spectral absorption for clear sky conditions.

We obtain a parameterization for the major absorption processes in the stratosphere, in the troposphere, and at the earth's surface. In this approach the formulas and coefficients are based in part on accurate multiple-scattering computations for specific model atmospheres. The parameterization is a function of the water vapor distribution, the amount and type of clouds, the zenith angle of the sun, the albedo of the earth's surface, and the ozone distribution. With this treatment of solar radiation the global atmospheric model at the Goddard

---

[1] Such as the cloud optical thickness, the extent to which the clouds are broken, the water vapor and ozone distributions, the gaseous absorption coefficients, the reflection function of the ground, etc.
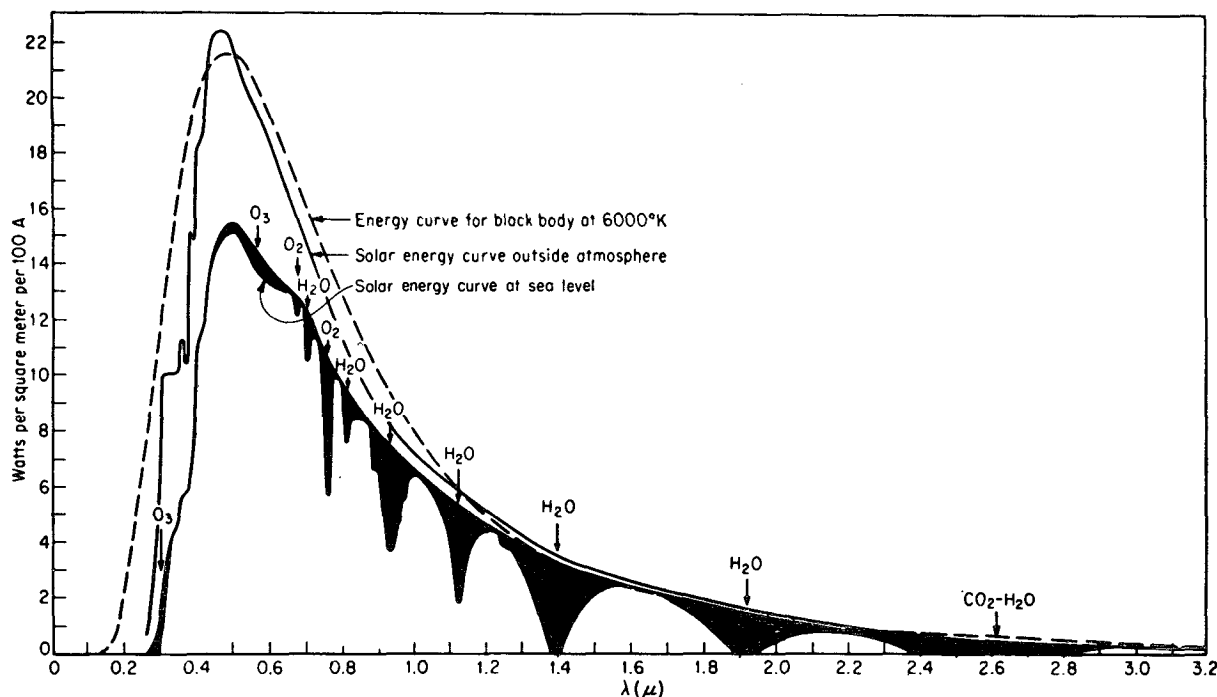
Fig. 1. Spectral energy curve of solar radiation at sea level and extrapolated outside the atmosphere, as given by Pettit (1951). The darkened areas represent gaseous absorption in the atmosphere.

Institute for Space Studies (Somerville *et al.*, 1974a) is being used to study possible effects of changes in the solar flux and the atmospheric composition.

In Section 2 we describe the multiple-scattering method which we use for making accurate monochromatic computations. In the later sections we present the results of computations for the major absorbers along with the parameterizations which we deduce.

2. Multiple-scattering method

We make computations for the absorption of solar radiation in a plane-parallel model atmosphere. The atmosphere is allowed to be vertically inhomogeneous and is divided into a sufficient number of layers (~ 50 for the more accurate computations) that each may be approximated as being homogeneous. The monochromatic scattering properties of each homogeneous layer are determined by its optical thickness τ, albedo for single scattering $\tilde{\omega}_0$, and phase function $p(\alpha)$, where α is the scattering angle.

The basic method of computation which we use is the "adding" method; this becomes the "doubling" method in the case of a homogeneous atmosphere or layer. The origins of this method date at least to the work of Peebles and Plesset (1951) in gamma-ray transfer. A similar approach was contained in the formalism of Redheffer for transmission-line theory; this work was done at about the same time as that of Peebles and Plesset (cf. Redheffer, 1962). van de Hulst

(1963) developed the method in essentially the form which we use.

Consider a plane-parallel layer of optical thickness τ illuminated uniformly from above by a parallel beam of radiation with flux πF_0 per unit area perpendicular to the incident beam. It is convenient to specify the intensity of radiation diffusively reflected and transmitted by the layer, I_r and I_t, in terms of reflection and transmission functions[2]:

$$\left. \begin{array}{l} I_r(\mu) = \mu_0 R(\mu,\mu_0) F_0 \\ I_t(\mu) = \mu_0 T(\mu,\mu_0) F_0 \end{array} \right\}, \qquad (1)$$

where $\theta_0 = \cos^{-1}\mu_0$ and $\theta = \cos^{-1}\mu$ are the angles of incidence and emergence, measured from the normal to the layer (Fig. 2). If the same layer is illuminated from below, the reflection and transmission functions are in general different than in the case of illumination from

---

[2] We neglect both the polarization and the azimuth dependence of the radiation. The omission of polarization is an approximation which introduces errors in the intensity of $\lesssim 10\%$ for Rayleigh scattering (Chandrasekhar, 1960) and $\lesssim 1\%$ for scattering by clouds (Hansen, 1971b). However, the quantity which we want in this paper is the energy (flux) absorbed in each layer; this requires integrations of the intensity over the upward and downward hemispheres which reduce the error to $\lesssim 0.1\%$, as shown by computations which we have made with and without polarization. The omission of azimuth dependence does not introduce any error since the amount of absorbed energy depends only on the first term in a Fourier expansion of the intensity.
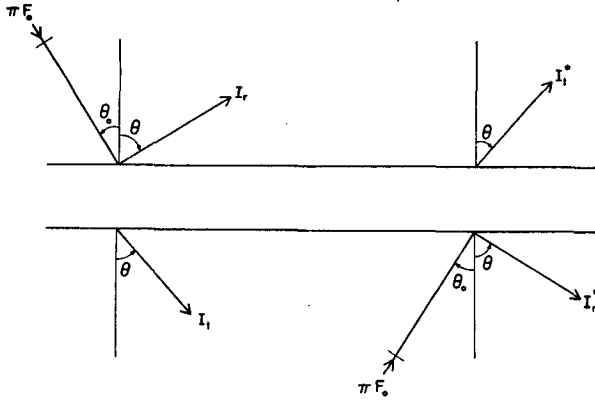
FIG. 2. Illustration of the angles of incidence (θ_0) and emergence (θ) for the reflection and transmission of radiation by a plane-parallel layer.

above and are denoted by R^* and T^* (Fig. 2):

$$\left.\begin{aligned} I_r^*(\mu) &= \mu_0 R^*(\mu,\mu_0) F_0 \\ I_t^*(\mu) &= \mu_0 T^*(\mu,\mu_0) F_0 \end{aligned}\right\}. \qquad (2)$$

The adding method provides a prescription for obtaining the reflection and transmission functions for a composite layer formed by combining two layers one on top of the other. Let the subscripts a and b refer to the top and bottom layer respectively. The procedure is then

$$\left.\begin{aligned} Q_1 &= R_a^* R_b \\ Q_n &= Q_1 Q_{n-1} \\ S &= \sum_{n=1}^{\infty} Q_n \\ D &= T_a + S \exp(-\tau_a/\mu_0) + S T_a \\ U &= R_b \exp(-\tau_a/\mu_0) + R_b D \\ R(\tau_a+\tau_b) &= R_a + \exp(-\tau_a/\mu) U + T_a^* U \\ T(\tau_a+\tau_b) &= \exp(-\tau_b/\mu) D \\ &\quad + T_b \exp(-\tau_a/\mu_0) + T_b D \end{aligned}\right\} . \qquad (3)$$

The physical basis for this prescription can be inferred from Fig. 3. The exponential terms refer to *direct* transmission through layer a or b without scattering; T is the *diffuse* transmission. Emerging from the bottom of the two layers is the diffuse transmission $T(\tau_a+\tau_b)$ and the unscattered radiation of flux $\pi F_0 \exp[-(\tau_a+\tau_b)/\mu_0]$ in the direction θ_0. We explicitly divide the transmission into its diffuse and direct components because the appearance of a delta function in the total transmission makes it inappropriate for precise numerical integrations. The indicated summation is over the reflections between the two layers with n indicating the number of times the radiation has crossed the dividing boundary going up.

In (3) a single upper case letter represents a function of two angles; thus,

$$Q_1 \equiv Q_1(\mu,\mu_0).$$

The product of two functions implies an integration over the adjoining angle as follows:

$$R_a^* R_b \equiv 2 \int_0^1 R_a^*(\mu,\mu') R_b(\mu',\mu_0) \mu' d\mu'.$$

Here D and U are the downward and upward diffuse intensities at the interface between the two layers. In practice, the sum in (3) may be terminated after a few terms (Hansen, 1971a). We perform the integrations over angle numerically using Gauss quadrature, i.e.,

$$Q_1(\mu_i,\mu_j) \approx \sum_{k=1}^{N_g} R_a^*(\mu_i,\mu_k) R_b(\mu_k,\mu_j) w_k \left\{\begin{aligned} i &= 1, N_g+N_x \\ j &= 1, N_g+N_x \end{aligned}\right.$$

The w_k are twice the Gauss weights for the interval (0,1). The number of Gauss divisions, N_g, is typically 5–25, depending on the anisotropy of the phase function and on the required accuracy of the results. For a given accuracy requirement the number of Gauss points can be reduced by employing a renormalization of the phase function (Hansen, 1971b). N_x is the number of angles, in addition to the Gauss divisions, for which results are desired.

We find R^* and T^* by using a computational scheme analogous to (3):

$$\left.\begin{aligned} Q_1 &= R_b R_a^* \\ Q_n &= Q_1 Q_{n-1} \\ S &= \sum_{n=1}^{\infty} Q_n \\ U &= T_b^* + S \exp(-\tau_b/\mu_0) + S T_b^* \\ D &= R_a^* \exp(-\tau_b/\mu_0) + R_a^* U \\ R^*(\tau_a+\tau_b) &= R_b^* + \exp(-\tau_b/\mu) D + T_b D \\ T^*(\tau_a+\tau_b) &= \exp(-\tau_a/\mu) U \\ &\quad + T_a^* \exp(-\tau_b/\mu_0) + T_a^* U \end{aligned}\right\} . \qquad (4)$$

Although the same notation is used for intermediate results (Q_1, Q_n, S, U, D) in (3) and (4), the numerical values are not necessarily identical. We do not actually need to compute the last line in (4) because, with polarization and azimuth-dependence neglected, $T^*(\mu,\mu_0) = T(\mu_0,\mu)$ [Hovenier, 1969].

The ground is "added" to the atmosphere, as if it were another layer, with the following specifications: $T_{L+1} = 0$, since no light is transmitted, and $R_{L+1} = R_g(\mu,\mu_0)$, the reflection function of the ground in the absence of an atmosphere. If the ground is approximated as a Lambert reflector, R_g is a constant between
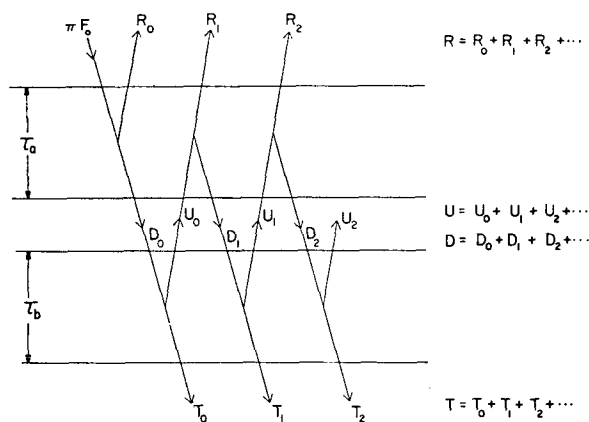
$$\pi F_0 \quad R_0 \quad R_1 \quad R_2$$

$$R = R_0 + R_1 + R_2 + \cdots$$

$$\tau_a$$

$$U_0 \quad U_1 \quad U_2$$
$$D_0 \quad D_1 \quad D_2$$

$$U = U_0 + U_1 + U_2 + \cdots$$
$$D = D_0 + D_1 + D_2 + \cdots$$

$$\tau_b$$

$$T_0 \quad T_1 \quad T_2$$

$$T = T_0 + T_1 + T_2 + \cdots$$

FIG. 3. Schematic representation of the adding method. The two layers of the atmosphere, of optical thickness τ_a and τ_b, are for convenience illustrated as if they were physically separated. The top layer is uniformly illuminated from above by parallel radiation of flux πF_0. The total radiation reflected by the two-layer atmosphere is the sum of terms corresponding to radiation which has crossed the boundary between the two layers n times going upward ($n=0$, ∞); the same is true for the diffusely transmitted radiation. In the actual computations [Eqs. (3)] it is only necessary to make one summation over n.

0 and 1. The total reflectivity (or albedo), which is the fraction of the incident energy reflected by the atmosphere and ground, is given by

$$\bar{R}(\mu_0) = 2 \int_0^1 R(\mu,\mu_0)\mu d\mu, \tag{5}$$

where $R(\mu,\mu_0)$ is the reflection function of the atmosphere plus ground. The total energy absorbed in the atmosphere and ground is $A(\mu_0) = 1 - \bar{R}(\mu_0)$.

In order to find how the absorbed energy is distributed among the individual layers of the atmosphere it is necessary to evaluate the internal fluxes between the individual layers. For this purpose we use the following scheme (cf. Fig. 4):

1) We compute R_l and T_l, $l=1$, L, where L is the total number of atmospheric layers, for each (homogeneous) layer of the atmosphere using the doubling method.[3] Note that $R_l^* = R_l$ and $T_l^* = T_l$.

2) Layers are added one at a time, going down, to obtain $R_{1,l}$ and $T_{1,l}$ for $l=2$, $L+1$ and $R_{1,l}^*$ and $T_{1,l}^*$ for $l=2$, L. For example, $R_{1,l}$ is the reflection function

---

[3] The doubling method consists of adding identical layers together to geometrically build up a thicker layer. The equations are the same as for the adding method [(3)], with $\tau_a = \tau_b$, $R_a = R_b$, $T_a = T_b$. The reflection and transmission functions of the initial layer may be obtained from single scattering equations (e.g., Hansen, 1971a), which requires an initial optical thickness $\tau_0 \approx 2^{-20}$, from single-plus-second-order scattering (Hovenier, 1971), which requires $\tau_0 \approx 2^{-15}$, or any other method. In our computations for an inhomogeneous atmosphere we use the doubling method for each homogeneous layer and the adding method to combine the layers. For brevity we sometimes refer to this as simply the doubling method.
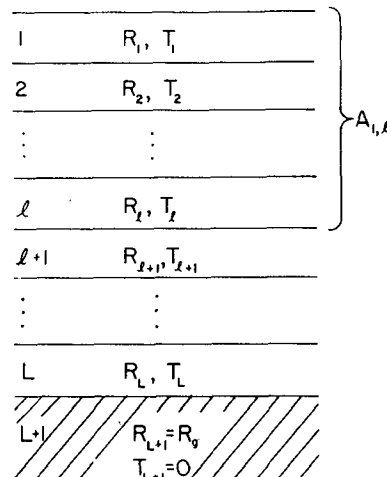

FIG. 4. Illustration of the terms used in the computation of absorption. The atmosphere is divided into a sufficient number of layers so that each may be taken as being homogeneous. The reflection and transmission properties of each layer are represented by two functions, R and T. The absorption in the composite of layers 1 through l is computed for all values of l as indicated in the text, and the absorption in the individual layers is then obtained by differencing.

for the composite of layers 1 through l with the lower part of the atmosphere and the ground absent.

3) Layers are added one at a time, going up, to obtain $R_{L+1-l,L+1}$, $l=1$, $L-1$. The process is started with the ground layer, for which $R_{L+1} = R_g$ and $T_{L+1} = 0$. After each layer is added, step 4) is performed.

4) The composite layers $(1,l)$ and $(l+1, L+1)$ are "added" to obtain the upward and downward intensities, $U_l(\mu,\mu_0)$ and $D_l(\mu,\mu_0)$, at the boundary between these two layers. The corresponding values for the relative flux[4] are given by

$$\left. \begin{array}{l} \bar{U}_l(\mu_0) = 2 \int_0^1 U(\mu,\mu_0)\mu d\mu \\[2mm] \bar{D}_l(\mu_0) = 2 \int_0^1 D(\mu,\mu_0)\mu d\mu \end{array} \right\}. \tag{6}$$

From these the fraction of the incident flux absorbed in the upper composite layer is obtained:

$$A_{1,l}(\mu_0) = 1 - \bar{R}(\mu_0)$$
$$+ \bar{U}_l(\mu_0) - \bar{D}_l(\mu_0) - \exp(-\tau_{1,l}/\mu_0), \tag{7}$$

where $\tau_{1,l}$ is the optical thickness of the composite layer $(1,l)$.

5) The absorption in the individual layers is found by differencing, e.g., $A_2 = A_{1,2} - A_1$, $A_3 = A_{1,3} - A_{1,2}$, etc.

3. Ozone absorption

Absorption of solar radiation by ozone is the major source of heating in the stratosphere (see, e.g., Manabe

---

[4] To obtain an absolute flux, $\bar{U}_l$ and $\bar{D}_l$ must be multiplied by $\mu_0 \pi F_0$.

and Strickler, 1964; Hering et al., 1967). This energy source should be included in numerical circulation models which include one or more layers above ~15 km.

Absorption by ozone can be accurately parameterized because the significant absorption occurs high in the atmosphere where there is little scattering.[5] Most of the scattering by air molecules (Rayleigh scattering) takes place below the ozone layer, so that the lower atmosphere acts mainly as a reflecting layer. Thus, the absorption of the direct solar beam and of the diffuse radiation reflected upward by the lower atmosphere and ground is primarily exponential attenuation at each wavelength. This has been recognized in the work of Craig (1951). However, the importance of including the effect of Rayleigh scattering in computing ozone heating rates has been noted by Herman and Yarger (1966) and by Dave and Furukawa (1967). In this paper, we provide increased accuracy for calculating ozone heating rates through simple formulas which explicitly include the effects of Rayleigh scattering and ground albedo.

Fig. 5 shows the solar flux outside the atmosphere according to Labs and Neckel (1968).[6] Also shown is the resulting spectral flux distribution after simple absorption by various amounts of ozone.[7] A typical amount in a vertical column of the atmosphere is 0.4 cm, NTP; at most times and locations on the earth the amount is between 0.2 and 0.6 cm (Prabhakara et al., 1971). Larger ozone amounts are encountered by the solar beam as the zenith angle increases.

The variation of absorption with ozone amount is much different in the weak visual (Chappuis) band than in the ultraviolet (Hartley and Huggins) bands. In Fig. 6 the percent of the solar flux absorbed as a function of ozone amount is explicitly compared for the two spectral regions. The ultraviolet bands appear practically saturated for 0.5 cm of ozone, while the visual absorption remains nearly proportional to the ozone amount. Note that the energy absorbed in the visual exceeds that in the ultraviolet for ozone paths greater than ~1 cm.

The first step in parameterizing ozone absorption in the atmosphere is to find analytical expressions for the frequency-integrated absorption curves of Fig. 6 as a function of ozone amount. For visual light the fraction of the incident solar flux that is absorbed by the

Chappuis band is given by

$$A_{oz}^{vis}(x) = \frac{0.02118x}{1+0.042x+0.000323x^2}, \qquad (8)$$

with a numerical precision of nearly four decimals in the interval 10^{-4} cm $\leqslant x \leqslant 10$ cm (NTP). The ultraviolet absorption is more difficult to fit. The expression

$$A_{oz}^{uv}(x) = \frac{1.082x}{(1+138.6x)^{0.805}} + \frac{0.0658x}{1+(103.6x)^3} \qquad (9)$$

gives the fraction of the solar flux absorbed in the ultraviolet with a maximum error $\lesssim 0.5\%$ in the interval 10^{-4} cm $\leqslant x \leqslant 1$ cm. It must, of course, be recognized that the above expressions[8] were obtained by integrating the solar flux and the ozone transmissivity over wavelength, so the absolute accuracy of the absorption is also limited by the imprecision in our knowledge of the solar flux and ozone absorption coefficients. Although some applications may require separate parameterization for ultraviolet and visual absorption, we are interested in the total absorption,

$$A_{oz}(x) = A_{oz}^{uv}(x) + A_{oz}^{vis}(x). \qquad (10)$$

The next step in the parameterization is to obtain a parametric formula for the absorption of the direct (unscattered) solar beam and the diffuse radiation reflected by the ground and lower atmosphere, with the coefficients of this formula defined through comparison with precise results computed with the doubling and adding method described in Section 2.

The ozone amount traversed by the direct solar beam in reaching the lth layer of the atmosphere is

$$x_l = u_l M, \qquad (11)$$

where u_l is the ozone amount in a vertical column above the lth layer, and

$$M = \frac{35}{(1224\mu_0^2+1)^{\frac{1}{2}}} \qquad (12)$$

is the magnification factor (Rodgers, 1967) accounting for the slant path and refraction. The ozone path traversed by the diffuse radiation illuminating the lth layer from below is

$$x_l^* = u_l M + \bar{M}(u_t - u_l), \qquad (13)$$

where u_t is the total ozone amount in a vertical path

---

[5] Also, the temperature and pressure dependence of the absorption coefficient is not very large and can be neglected if the coefficients are chosen for a temperature representative of the ozone layer.

[6] Integrated over all wavelengths their data yields a solar constant $\pi F_0 = 0.1365$ W cm^{-2} sec^{-1} (1.958 cal cm^{-2} min^{-1}).

[7] The absorption coefficients used in the computations were taken from Howard et al. (1961), the original sources being Inn and Tanaka (1953) and Vigroux (1953). In the ultraviolet, where the absorption has a significant temperature dependence, the coefficients for $T = -44$C were used; for wavelengths where these data were not given ($\lambda \gtrsim 0.34 \mu$m) the coefficients for $T = 18$C were used after reduction by 25%.

[8] The coefficients in the formulas were evaluated by means of an iterative least-square procedure utilizing the Fibonacci search technique (Napier, 1970). The coefficients were determined numerically using ~100 points to fit the results of precise integration over the specified intervals. In selecting the algebraic form of the formulas our aim was to find simple expressions giving satisfactorily high accuracy and having desirable asymptotic behavior outside the fitting interval.
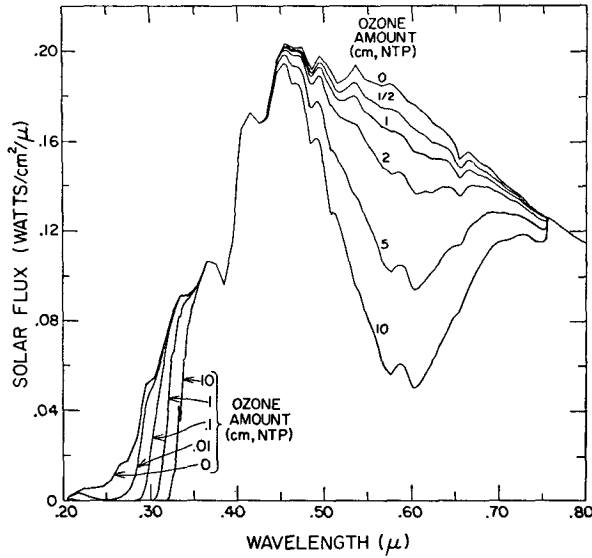
FIG. 5. Spectral distribution of solar flux outside the earth's atmosphere, and as calculated for transmission through various ozone amounts without scattering. The solar flux outside the earth's atmosphere (0 cm ozone) was taken from Labs and Neckel (1968) and the ozone absorption coefficients from Howard et al. (1961).

above the main reflecting layer (the ground for clear sky conditions, or the cloudtop for cloudy skies) and $\bar{M} = 1.9$ is the effective magnification factor for diffuse upward radiation.[9]

We model the ozone absorption in the atmosphere in terms of a purely absorbing region on top of a reflecting region. The parametric formula giving the fraction of the total solar flux absorbed in the lth layer of the atmosphere is then

$$A_{l,\text{oz}} = \mu_0\{A_{\text{oz}}(x_{l+1}) - A_{\text{oz}}(x_l)$$

$$+\bar{R}(\mu_0)[A_{\text{oz}}(\overset{*}{x_l}) - A_{\text{oz}}(\overset{*}{x_{l+1}})]\}, \quad (14)$$

where $\bar{R}(\mu_0)$ is the albedo of the reflecting region. $\bar{R}(\mu_0)$ includes the effective albedo of the lower atmosphere, $\bar{R}_a(\mu_0)$, and the ground reflectivity, R_g, as follows:

$$\bar{R}(\mu_0) = \bar{R}_a(\mu_0) + [1 - \bar{R}_a(\mu_0)](1 - \bar{\bar{R}}_a^*)R_g/(1 - \bar{\bar{R}}_a^* R_g). \quad (15)$$

In (15) it is implicitly assumed that the lower atmosphere is primarily a scattering region with negligible absorption. As shown later, this is indeed a good approximation. This assumption makes it possible to keep the form of the parameterization simple and to treat

the lower atmosphere as a homogeneous layer. Thus, in (15), $\bar{\bar{R}}_a^* = \bar{R}_a$, where

$$\bar{\bar{R}}_a = 2\int_0^1 \bar{R}_a(\mu_0)\mu_0 d\mu_0 \quad (16)$$

is the spherical albedo of the reflecting region, i.e., the average of $\bar{R}_a(\mu_0)$ over all sun angles. The denominator in the last term of (15) accounts for multiple reflections between the atmosphere and ground, with the approximation of isotropic reflection by the ground.

The parameterization of ozone absorption is completed by specifying the effective magnification factor $\bar{M}$ in (13) for the upward diffuse radiation and the effective albedo $\bar{R}_a(\mu_0)$ of the lower atmosphere. For the purpose of determining $\bar{M}$ and $\bar{R}_a(\mu_0)$ we have made computations using the analytic ozone distribution of Green (1964):

$$u(h) = \frac{a + a\exp(-b/c)}{1 + \exp[(h-b)/c]}, \quad (17)$$

where $u(h)$ is the ozone amount (cm, NTP) in a vertical column above the altitude h, a is the total ozone amount in a vertical column above the ground, b the altitude at which the ozone concentration $(-du/dh)$ has its maximum, and $a[1+\exp(-b/c)]/(4c)$ the maximum ozone concentration. Fig. 7 illustrates Green's distribu-
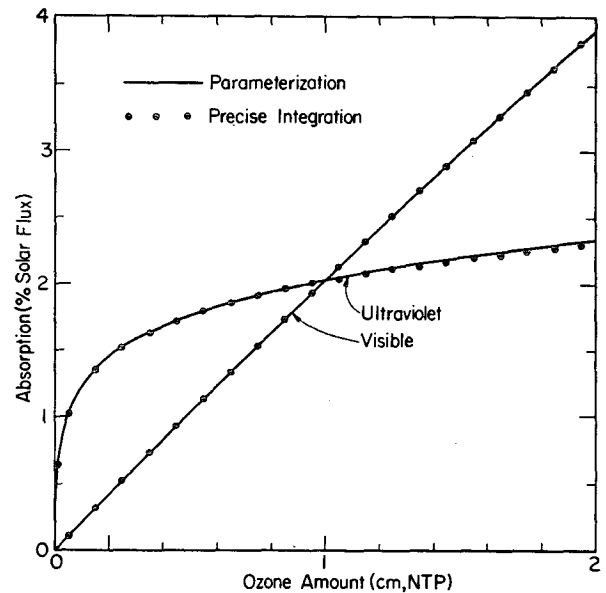

FIG. 6. Per cent of total solar flux absorbed as a function of ozone amount, for the spectral distribution of incident solar flux given by Labs and Neckel (1968) and the ozone absorption coefficients of Howard et al. (1961) at $-44C$. The dotted curves are the results of integrations over wavelength using the wavelengths at which Howard et al. tabulate the absorption coefficient. The analytic parameterization for the ultraviolet is given by (9) and that for the visual by (8).

---

[9] For isotropic radiation passing through a plane-parallel layer of optical thickness τ, $\bar{M}$ is a known function of $\tau[\exp(-\bar{M}\tau) = 2E_3(\tau)$, where E_3 is the third exponential integral; cf. pp. 18–19 and Fig. 1.3 of Kondratyev (1969)] ranging from $\bar{M}=2$ for $2E_3 = 1(\tau \to 0)$ to $\bar{M} = 1.2$ for $2E_3 = 0$ $(\tau \to \infty)$. The value $\bar{M} \approx 5/3$, valid for $2E_3 = \frac{1}{2}$, is often used if an accurate knowledge of τ is lacking. We obtained the value $\bar{M} = 1.9$ from multiple-scattering results, as described in this Section.
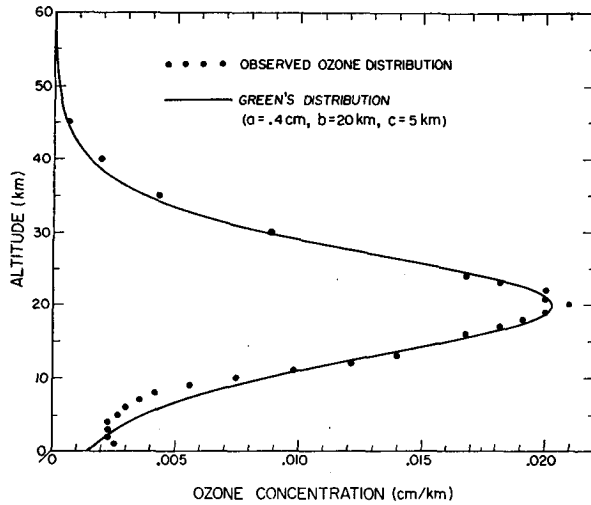
FIG. 7. Vertical ozone distribution. The dots are the distribution given by McClatchey et al. (1972) as typical for mid-latitude winter. The solid curve is the distribution (17), in which a is the total ozone amount in a vertical column and b the altitude of maximum concentration.

tion with $a=0.4$ cm, $b=20$ km and $c=5$ km; this is a close fit to the mid-latitude winter ozone distribution tabulated by McClatchey et al. (1972).

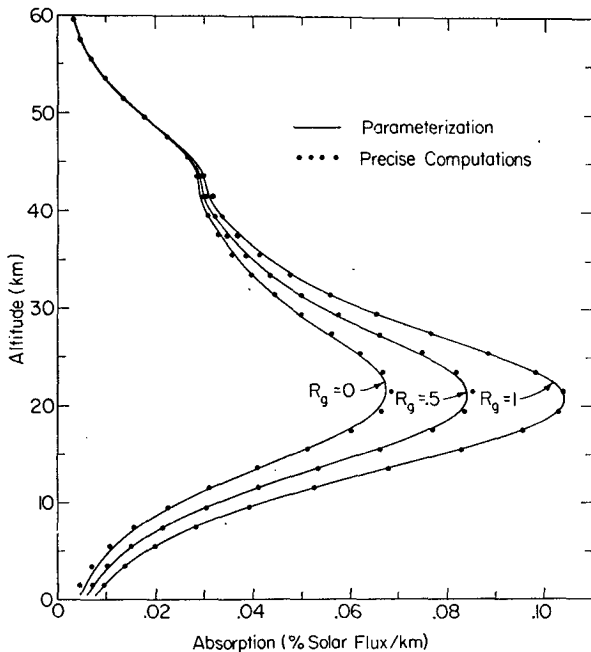The numerical value for $\bar{M}$ was determined by varying it to find the best fit in a least-squares sense to

FIG. 8. Absorption of solar radiation by ozone, for the solar zenith angle $\theta_0=60°$ and three values of the ground albedo R_g. The distribution of Rayleigh scatterers was taken from the U. S. Standard Atmosphere (Champion et al., 1962) and the ozone distribution from (17), for $a=0.4$ cm, $b=20$ km and $c=5$ km; no clouds or aerosols are included. The parameterizations were obtained from (14) and the precise computations as described in Section 2.

multiple-scattering results for a clear sky (Rayleigh atmosphere), both as a function of height and for different zenith angles. We did this by first setting $R_g=1$ which removed the dependence of (14) on the atmospheric albedo [i.e., $\bar{R}(\mu_0)=1$ in (14)] and left M as the only adjustable parameter. Comparison between the parametric formula (14) and the doubling (and adding) method was made for a 60-layer atmosphere with 8 different zenith angles used in the computations. Each layer was taken to be 1 km thick with an additional single layer included for heights >60 km. In the fitting process less weight was given to the absorption curves for zenith angles $>60°$ and heights <10 km. In Fig. 8 the curve for $R_g=1$ shows the result of the best fit with $\bar{M}=1.9$ for a zenith angle of 60°; the solid line was computed with (14) and the dots with the doubling method.

With $\bar{M}$ determined we put $R_g=0$, so that for clear skies the albedo of the lower atmosphere was due entirely to Rayleigh scattering. For each zenith angle used in the computations (μ_i) an effective albedo $[\bar{R}(\mu_i)]$ was obtained by iterative least-square fitting which gave the best agreement between the vertical absorption profiles for the parametric formula (14) and the doubling method. Then, from a least-square fit to the individual $\bar{R}(\mu_i)$, we obtained

$$\left.\begin{array}{l} \bar{R}_a(\mu_0)=\dfrac{0.219}{1+0.816\mu_0} \\[2mm] \bar{\bar{R}}_a^{*}=\bar{\bar{R}}_a=0.144 \end{array}\right\}\text{[clear skies]}. \qquad (18)$$

In terms of the reflecting layer model used to parameterize the ozone absorption, Eq. (18) represents the effective albedo of the lower atmosphere due to Rayleigh scattering. This should not, however, be confused with the albedo of the Rayleigh atmosphere given by Eq. (41) in Section 5. The accuracy of our analytic fit to the absorption for Rayleigh scattering is shown by the $R_g=0$ curve in Fig. 8 for a zenith angle of 60°.

For cloudy skies we neglect the effect of Rayleigh scattering and use the following two-stream approximation for the cloud albedo:

$$\bar{R}_a(\mu_0)=\bar{\bar{R}}_a=\frac{\sqrt{3}(1-g)\tau^c}{2+\sqrt{3}(1-g)\tau^c}$$

$$\approx\frac{0.13\tau^c}{1+0.13\tau^c} \qquad \text{[cloudy skies]}, \qquad (19)$$

where τ^c is the total visual optical thickness of the clouds and we have used $g\approx0.85$ as the asymmetry factor for the cloud particle phase function (Hansen and Pollack, 1970). We obtained (19) by taking the limit $\tilde{\omega}_0\to1$ in the more general two-stream equation (31). Since (19) refers to a homogeneous scattering layer, $\bar{\bar{R}}_a^{*}=\bar{\bar{R}}_a$.
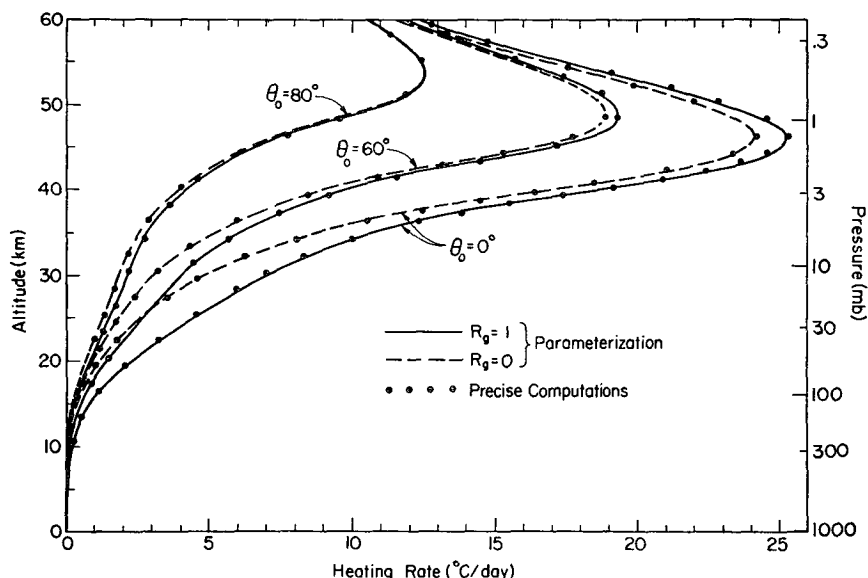
Fig. 9. Heating rate due to absorption of solar radiation by ozone, for three values of the solar zenith angle θ_0, and two values of the ground albedo R_g. The ozone distribution is that given by (17) with $a=0.4$ cm, $b=20$ km and $c=5$ km.

Fig. 8 illustrates that most of the ozone absorption takes place near the maximum ozone concentration, where it is primarily due to the visual Chappuis band and the longer ultraviolet wavelengths of the Huggins band. Because the visual absorption coefficient is small, the absorption of the direct solar beam by the Chappuis band is proportional to the ozone concentration and is nearly independent of the zenith angle. The visual absorption is also very sensitive to the ground albedo. For moderate zenith angles and typical cloud albedos the absorbed energy due to the diffuse reflected radiation can exceed that of the direct solar beam. The ultraviolet absorption, however, is practically independent of ground albedo. Except for the longer wavelengths of the Huggins band, very little of the direct ultraviolet solar beam actually penetrates to the ground. Most of the absorption in the ultraviolet occurs at altitudes 25-50 km, above the region of maximum ozone concentration. The ultraviolet absorption depends strongly on the zenith angle except for heights $\gtrsim 50$ km, where the direct solar beam has not yet become saturated.

For meteorological purposes the heating rate is of more immediate interest than the absorbed energy. In the earth's atmosphere the heating rate is related to the absorbed energy by

$$\frac{\Delta T}{\Delta t} = \frac{\pi F_0 g A_l}{c_p \Delta P \Delta t}, \qquad (20)$$

where c_p is the specific heat at constant pressure, g the acceleration of gravity, ΔP the pressure difference between the top and bottom of the lth layer, and A_l the fraction of the total solar flux absorbed in the lth layer as given by (14) for ozone.

Heating rates due to ozone obtained for the mid-latitude winter ozone distribution ($a=0.4$ cm, $b=20$ km, $c=5$ km) are shown in Fig. 9 for extreme ground albedos, $R_g=0$ and 1, and three solar zenith angles, $\theta_0=0°$, $60°$ and $80°$. The maximum heating rate is at a much higher altitude than the ozone maximum, as a result of absorption by the strong ultraviolet band at altitudes where the density is low. Note that the heating rate due to absorption by ozone is very small for altitudes $\lesssim 10$ km. The effect of the ground albedo is significant for altitudes in the range ~ 10 km to ~ 35 km, as can also be seen from the calculations of Dave and Furukawa (1967).

Fig. 10 shows heating rates calculated for two additional ozone distributions: one is representative of equatorial conditions ($a=0.25$ cm, $b=25$ km, $c=4$ km), and the other polar winter conditions ($a=0.5$ cm, $b=18$ km, $c=4$ km). The results are qualitatively similar for these different distributions. Note, however, that the tropical distribution has the larger heating rate at high altitudes. Due to the greater altitude of the ozone maximum ($b=25$ km) the tropical distribution has the larger ozone amount at high altitudes. The heating rate for the polar distribution is much stronger in the region of ~ 20 km where the absorption is due mainly to the visual Chappuis band and the longer ultraviolet wavelengths of the Huggins band.

The calculations for the vertical ozone distributions serve to verify that the parameterization has a general validity. The distributions used for Fig. 10 cover a range of ozone amount representative of the real atmosphere, and the parameterization error remains practically identical to that for the ozone distribution
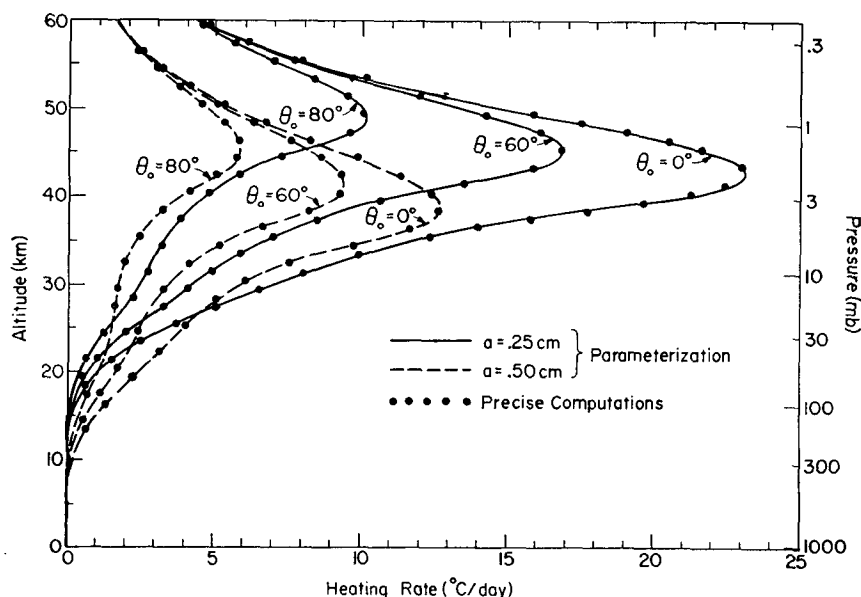
FIG. 10. Heating rate due to absorption of solar radiation by ozone, for three values of the solar zenith angle θ_0, and two ozone distributions. The distribution with $a=0.25$ cm has $b=25$ km, $c=4$ km, and is representative of equatorial conditions; while the distribution with $a=0.5$ cm has $b=18$ km, $c=4$ km, and is representative of polar winter conditions. The ground albedo is $R_g=0.5$ in all cases.

used in obtaining $\bar{M}$ and $\bar{R}_a(\mu)$. This indicates that $\bar{M}$ and $\bar{R}_a(\mu_0)$ are not very sensitive to the ozone amount. The ozone absorption in the atmosphere can thus be accurately described in terms of a purely absorbing and reflecting model, provided that multiple scattering is adequately accounted for, as it has been here, for example, in terms of the effective magnification factor and the effective Rayleigh albedo.

The accuracy of the ozone parameterization is typically within $\sim 1\%$ compared to results obtained with the doubling and adding method. Errors of $\sim 3\%$ occur at a height of 30–40 km due to inaccuracy of the ultraviolet absorption formula (9) for ozone paths of ~ 0.02 cm. Below ~ 15 km the parameterization tends to overestimate the absorption when the zenith angle becomes large. For $\theta_0=80°$ the error is $\sim 10\%$ at 10 km. This is because for large zenith angles the effect of scattering is to shorten rather than increase the effective path length of a light ray through the absorbing medium. Except for heights $\lesssim 10$ km, the ground albedo has little influence on the error in the parameterization.

4. Water vapor absorption

Absorption by water is the major source of solar radiative heating in the atmosphere. The parameterization of water vapor absorption is more difficult than that of ozone absorption because: 1) the absorption coefficient of water vapor is highly frequency-dependent and accurate monochromatic values are not available for the entire spectrum; 2) significant scattering and absorption can occur in the same part of the atmo-

sphere, precluding a simple reflecting model such as that used for ozone; and 3) the absorption coefficient has a significant dependence on pressure.

For clear skies the effect of scattering is negligible and the absorption due to water vapor is obtained directly from empirical absorption functions. For cloudy skies multiple scattering is the principal factor affecting the absorption; in this case, we base our parameterization on a discrete probability distribution for the absorption coefficient derived from measured absorptivities. In both cases a scaling approximation is used as a rough correction for the effect of pressure and temperature on the absorption. This approach allows realistic modeling of the effects of multiple scattering. However, because of the absence of monochromatic absorption coefficients and their pressure-temperature dependence, we have not yet made a full assessment of the accuracy of this method.

Absorption by major water vapor bands has been measured at low spectral resolution by Howard *et al.* (1956). Yamamoto (1962) weighted these absorptivities with the solar flux and summed them, including estimates for the weak absorption bands near 0.7 and 0.8 μm which were not measured by Howard *et al.*, to obtain the total absorption as a function of water vapor amount y (centimeters of precipitable water vapor). The formula

$$A_{wv}(y)=\frac{2.9y}{(1+141.5y)^{0.635}+5.925y} \qquad (21)$$

fits Yamamoto's absorption curve within $\lesssim 1\%$ for

$10^{-2} \leqslant y \leqslant 10$ cm. The water vapor absorptivity given by (21) is compared in Fig. 11 with the absorptivities of Fowle (1915) and Korb et al. (1956). The formula based on Fowle's old laboratory data,

$$A_{wv}(y) = 0.0946 y^{0.303}, \qquad (22)$$

includes a modification of $\sim 10\%$ introduced by Manabe and Möller (1961) to account for the bands at 0.7 and 0.8 μm; these weak bands contribute significant absorption because of the large solar flux in that region. The formula of Korb et al.,

$$\log_{10}[2A_{wv}(y)] = -0.74 + 0.347 \log_{10} y$$
$$-0.056 \log_{10}{}^2 y - 0.006 \log_{10}{}^3 y, \quad (23)$$

uses the Curtis-Godson approximation and is also based on the Howard et al. absorption data, but it does not include the weak near-infrared bands at 0.7 and 0.8 μm. Although the three curves in Fig. 11 are qualitatively similar, their differences are significant, particularly for small water vapor amounts. Moreover, the uncertainty in their absolute value is as great as the differences among the three curves.

The absorptivities (21)–(23) apply for standard pressure and temperature ($P_0 = 1013$ mb and $T_0 = 273$K). We make a common approximate correction for the pressure and temperature dependence of the absorption by using an effective water vapor amount,

$$y^{\text{eff}} = y \left(\frac{P}{P_0}\right)^n \left(\frac{T_0}{T}\right)^{\frac{1}{2}}. \qquad (24)$$
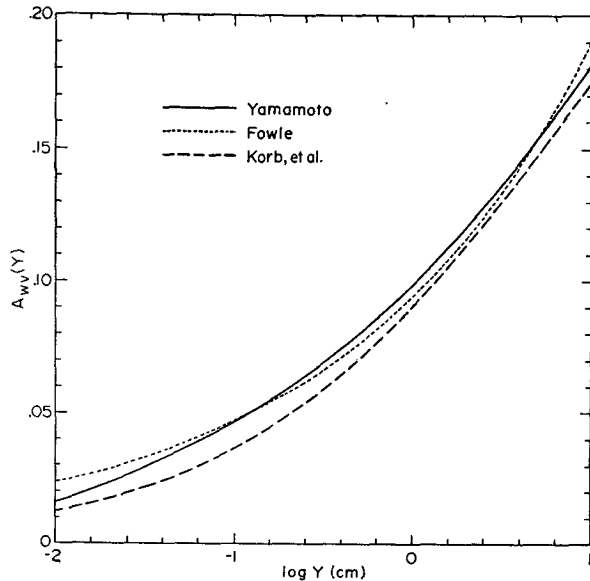
There is little theoretical justification for using (24)

Fig. 11. Absorptivity vs water vapor amount in precipitable centimeters, where absorptivity = 1 − transmission, and refers to the entire solar spectrum. The three curves are given by (21)–(23), and all refer to standard pressure and temperature.

for the entire spectrum of water vapor bands (cf. Goody, 1964), but it is probably better than applying no pressure and temperature correction at all.[10]

a. Clear skies

In the spectral regions of significant water vapor absorption the optical thickness of the atmosphere due to Rayleigh scattering is negligible. The absorption by water in the lth layer of the clear atmosphere is

$$A_{l,wv} = \mu_0 \pi F_0 \{ A_{wv}(y_{l+1}) - A_{wv}(y_l)$$
$$+ R_g [A_{wv}(\overset{*}{y_l}) - A_{wv}(\overset{*}{y_{l+1}})] \}. \qquad (25)$$

In the above R_g is the ground albedo; y_l is the effective water vapor amount traversed by the direct solar beam in reaching the lth layer,

$$y_l = \frac{M}{g} \int_0^{P_l} q \left(\frac{P}{P_0}\right)^n \left(\frac{T_0}{T}\right)^{\frac{1}{2}} dP; \qquad (26)$$

q is the specific humidity; g the acceleration of gravity; and y_l^* the effective water vapor amount traversed by the reflected radiation in reaching the lth layer from below,

$$\overset{*}{y_l} = \frac{M}{g} \int_0^{P_g} q \left(\frac{P}{P_0}\right)^n \left(\frac{T_0}{T}\right)^{\frac{1}{2}} dP$$
$$+ \frac{5}{3g} \int_{P_{l+1}}^{P_g} q \left(\frac{P}{P_0}\right)^n \left(\frac{T_0}{T}\right)^{\frac{1}{2}} dP, \qquad (27)$$

where P_l, P_{l+1} and P_g are the pressures at the top of the lth layer, at the bottom of the lth layer and at the ground. The average magnification factor for the diffuse radiation is taken to be 5/3.

Fig. 12 shows the clear sky heating rate due to water vapor absorption for a solar zenith angle of $\theta_0 = 60°$. The computations were made using a mid-latitude winter water vapor distribution tabulated by McClatchey et al. (1972); the amount of precipitable water vapor in the atmosphere is 0.86 cm, which corresponds to 0.7 cm for the linear ($n = 1$) scaling relation. The structure in the heating rate curves, including the bulges at altitudes of ~ 3 and ~ 6 km, arises primarily from the inhomogeneous vertical distribution of the water vapor. Fowle's absorptivity gives the largest heating rate in the upper troposphere, Yamamoto's the largest in the middle troposphere, and Korb et al.'s the largest in the lower troposphere. The relative differences

---

[10] Eq. (24) is an approximation used to compute absorption along a non-homogeneous path; the true water vapor amount along the non-homogeneous path is replaced by a scaled amount at a given pressure and temperature. In the weak-line limit, the absorption is independent of pressure, i.e., $n = 0$. In the strong-line limit, $n = 1$. In computing water vapor absorption in the earth's atmosphere the usual practice is to take n between 0.5 and 1.
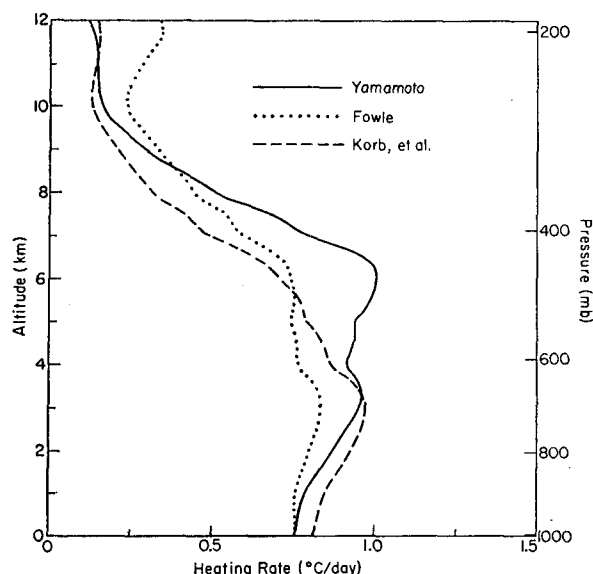
FIG. 12. Heating rate due to water vapor absorption in a clear sky with the solar zenith angle $\theta_0 = 60°$. The standard atmosphere and water vapor distribution of McClatchey *et al.* (1972) are assumed. The heating rates are computed from (20), (24) and (25) for the three absorptivities given by (21), (22) and (23). The ground albedo is $R_g = 0.07$, which is representative of mean ocean albedo.

tend to increase with increasing altitude. The ground albedo for Figs. 12–15 is $R_g = 0.07$ which is representative of the mean ocean albedo.

Fig. 13 illustrates the effect of pressure scaling on the heating rate due to water vapor absorption. The three
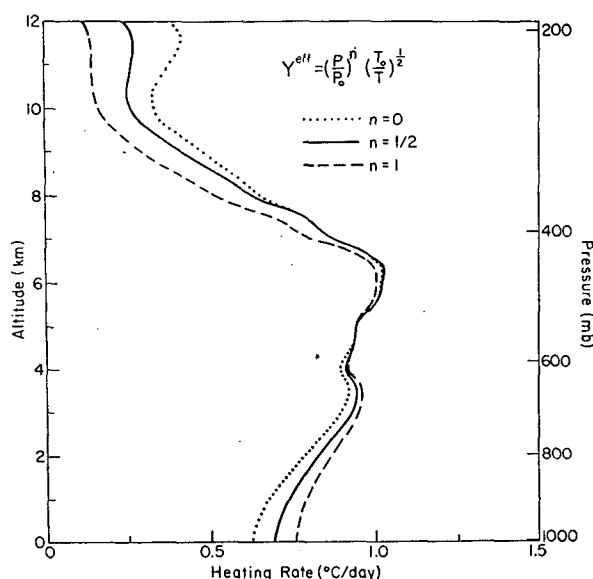

FIG. 13. The effect of pressure scaling on the heating rate in a clear sky. The solar zenith angle is $\theta_0 = 60°$ and the standard atmosphere and water vapor distribution of McClatchey *et al.* (1972) are assumed. The computations use Yamamoto's absorptivity (21). The ground albedo is $R_g = 0.07$.

curves for $n = 0$, 0.5 and 1 show that the principal effect of pressure scaling is to reduce the heating rate in the upper troposphere. Near the ground the order of the curves is reversed because the transmitted flux is larger for the stronger pressure scaling, while the effective water vapor amounts are nearly identical for all three curves. The difference between the curves for $n = 0.5$ and $n = 1$ is perhaps a rough measure of the uncertainty in the water vapor heating rate due to the scaling approximation. Although this uncertainty is large at high altitudes, it should be remembered that the relative contribution of water vapor heating to the total solar heating decreases with altitude as heating by other gases, particularly O_3, increases (cf. Manabe and Möller, 1961; Sasamori *et al.*, 1972).

Recent aircraft measurements of the vertical profile of the net solar flux made by Paltridge (1973) are in good agreement with Yamamoto's absorptivity. Although the measurements refer to altitudes $\lesssim 4$ km, they indicate that a linear pressure scaling for water vapor amount is significantly better than no scaling at all. The calculations in the remainder of this paper employ Yamamoto's water vapor absorptivity (21) with linear pressure scaling. The square-root temperature scaling is also used, as indicated in (26) and (27), but its effect is small and less than the magnitude of the other uncertainties.

b. Cloudy skies

To calculate the absorption for cloudy skies we use approximate multiple-scattering computations in conjunction with a probability distribution,[11] $p(k)$, for the absorption coefficient. The expression $p(k)dk$ is the fraction of the incident flux that is associated with an absorption coefficient between k and $k+dk$, and it is related to the absorptivity by

$$A_{wv}(y) = 1 - \int_0^\infty p(k)e^{-ky}dk. \qquad (28)$$

Replacing the integral by a finite sum, i.e.,

$$\int p(k)e^{-ky}dk \approx \sum_{n=1}^N p(k_n)e^{-k_n y}. \qquad (29)$$

Eq. (28) can be numerically inverted to obtain N values for the discrete probability distribution $p(k_n)$ and N values for the corresponding absorption coefficient k_n. Table 1 gives the values of k_n and $p(k_n)$ for $N = 8$ which fit the Yamamoto absorptivity (21) within 0.1% for 10^{-2} cm $< y < 10$ cm. The accuracy of the fit for the derivative dA/dy, which is proportional to the heating rate, is within $\sim 1\%$ for the same interval. The numerical inversion was performed by means of an itera-

---

[11] Probability functions for the absorption coefficient have been used by a number of authors in problems not involving multiple scattering, e.g., by Kondratyev (1969) and Arking and Grossman (1972).

tive least square search similar to that described in Section 3.

To calculate the absorption by water vapor in a cloudy atmosphere we use an adaptation of the adding method described in Section 2. The atmosphere is divided in L homogeneous layers. The optical properties of each layer are specified by the total optical thickness τ of the layer and by the single scattering albedo $\tilde{\omega}$:

$$\left. \begin{array}{l} \tau_{l,n} = \tau_l^c + k_n w_l \\ \tilde{\omega}_{l,n} = \tau_l^c / \tau_{l,n} \end{array} \right\}, \qquad (30)$$

where τ_l^c is the optical thickness due to cloud particles in the lth layer and w_l the effective water vapor amount in a vertical path through the lth layer.

The reflection and transmission functions[12] for each cloud layer are approximated with two-stream equations (Sagan and Pollack, 1967):

$$\left. \begin{array}{l} R_l = \dfrac{(u+1)(u-1)(e^t - e^{-t})}{(u+1)^2 e^t - (u-1)^2 e^{-t}} \\[2ex] T_l = \dfrac{4u}{(u+1)^2 e^t - (u-1)^2 e^{-t}} \\[2ex] u = \left(\dfrac{1 - g\tilde{\omega}_{l,n}}{1 - \tilde{\omega}_{l,n}} \right)^{\frac{1}{2}} \\[2ex] t = [3(1 - \tilde{\omega}_{l,n})(1 - g\tilde{\omega}_{l,n})]^{\frac{1}{2}} \tau_{l,n} \end{array} \right\}. \qquad (31)$$

We use $g = 0.85$ for the asymmetry factor for clouds (Hansen and Pollack, 1970). Note that for a homogeneous cloud layer $R_l^* = R_l$ and $T_l^* = T_l$, where the asterisk indicates illumination from the bottom side of the layer.

The reflection and transmission functions for a *clear layer* are taken to be

$$R_l = R_l^* = 0, \qquad (32a)$$

$$T_l = T_l^* = \exp(-5\tau_{l,n}/3), \qquad (32b)$$

except for a clear layer above the highest cloud layer, for which

$$T_l = \exp(-M\tau_{l,n}). \qquad (32c)$$

Thus, all radiation reflected or transmitted by a cloud is assumed to be diffuse with an average magnification factor 5/3.

The reflection and transmission functions for a composite layer formed by adding two layers are

$$\left. \begin{array}{l} R_{ab} = R_a + T_a R_b T_a^* / (1 - R_a^* R_b) \\ T_{ab} = T_a T_b / (1 - R_a^* R_b) \end{array} \right\}, \qquad (33)$$

---

[12] In this Section the transmission function is taken as including both the diffuse and direct transmission.

TABLE 1. Discrete probability distribution of water vapor absorption coefficients for $N = 8$.

n	k_n	$p(k_n)$
1	4×10^{-5}	0.6470
2	0.002	0.0698
3	0.035	0.1443
4	0.377	0.0584
5	1.95	0.0335
6	9.40	0.0225
7	44.6	0.0158
8	190.	0.0087

where the subscripts a and b refer to the top and bottom layer, respectively. The denominator accounts for multiple reflections between the two layers. For illumination from below

$$\left. \begin{array}{l} R_{ab}^* = R_b^* + T_b^* R_a^* T_b / (1 - R_a^* R_b) \\ T_{ab}^* = T_b^* T_a^* / (1 - R_a^* R_b) \end{array} \right\}. \qquad (34)$$

The energy absorbed in each layer is calculated by a procedure analogous to that described in Section 2. The following five steps are carried out for each value of k_n which can yield significant absorption, e.g., $n = 2 - 8$ for the discrete distribution in Table 1.[13]

1) R_l and T_l, $l = 1$, L are computed for each layer by means of (31)–(32).

2) The layers are added, going down, to obtain $R_{1,l}$ and $T_{1,l}$ for $l = 2$, $L+1$ and $R_{1,l}^*$ and $T_{1,l}^*$ for $l = 2$, L.

3) Layers are added one at a time, going up, to obtain $R_{L+1-l,L+1}$, $l = 1$, $L-1$ starting with the ground layer, $R_{L+1} = R_g$ and $T_{L+1} = 0$. After each layer is added, step 4) is performed.

4) As two composite layers, say 1, l and $l+1$, $L+1$, are added, the upward and downward fluxes at the boundary between the two layers are determined:

$$\left. \begin{array}{l} U_l = T_{1,l} R_{l+1,L+1} / (1 - R_{1,l}^* R_{l+1,L+1}) \\ D_l = T_{1,l} / (1 - R_{1,l}^* R_{l+1,L+1}) \end{array} \right\}. \qquad (35)$$

The fraction of the total incident flux absorbed in the upper composite layer is

$$A_{1,l}(n) = p(k_n)[1 - R_{1,L+1}(n) + U_l(n) - D_l(n)]. \qquad (36)$$

5) The absorption in the individual layers is found by differencing, e.g.,

$$A_2(n) = A_{1,l}(n) - A_1(n). \qquad (37)$$

The total absorption in each layer l is found by summing over the values of n for which k_n is significant,

---

[13] To save computer time the absorption of the direct solar beam above the highest cloud can be computed from the absorptivity equation (21). Also, for large values of k_n the multiple-scattering computations can be stopped once the associated flux is depleted below a negligible fraction.
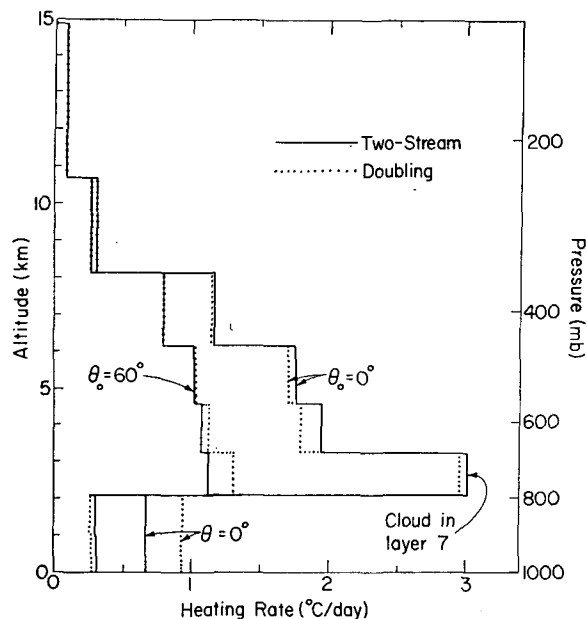
FIG. 14. Heating rates in the troposphere computed for water vapor absorption. A cloud of optical thickness $\tau^c=8$ is assumed to uniformly fill layer 7 in which the relative humidity is 100%. In other layers the standard atmosphere and water vapor distribution of McClatchey et al. (1972) is used. The layer boundaries are those for the 9-layer atmospheric model used by Somerville et al. (1974a) with a surface pressure 1013 mb. The solid lines represent the heating rates obtained with the parameterization described in the text. The dotted lines show the results obtained with the doubling and adding method, including accurate integrations over angle. The ground albedo is $R_g=0.07$.

i.e.,

$$A_l \approx \sum_n A_l(n). \qquad (38)$$

The solid histograms in Fig. 14 show heating rates due to water vapor absorption computed by the above method. For these computations the atmosphere was divided into nine homogeneous layers corresponding to the layers in the numerical circulation model described by Somerville et al. (1974a). A single cloud layer of optical thickness $\tau^c=8$ was assumed to fill layer 7, as indicated in Fig. 14. The mid-latitude winter water vapor distribution of McClatchey et al. (1972) was used, except in layer 7 where the relative humidity was assumed to be 100%.

Fig. 14 also shows the results obtained when the two-stream approximation is replaced by doubling and adding computations with accurate integrations over angle. The comparison serves primarily as a test for the angle integration aspect of the parameterization. The only large errors occur in the subcloud region. This can be traced to the simple two-stream formulas employed, which yield a cloud albedo independent of the solar zenith angle. A closer correspondence could be obtained if a more accurate treatment was used for the cloud albedo and transmission. However, for most

applications this is not necessary since the error tends to be averaged out with time as the zenith angle of the sun varies.

Fig. 15 shows the heating rates with clouds in different layers. The optical thickness τ^c for layers 5 and 7 is taken to be 8, corresponding approximately to altostratus and cumulus type clouds with visual albedos of $\sim 50\%$. The cloud in layer 3 with $\tau^c=2$ and a corresponding visual albedo of $\sim 20\%$ is typical of cirrus clouds. In the computations for this figure the atmosphere was divided into 45 layers to provide greater detail for the heating rate curves. The major effect of the clouds is to increase the heating within the clouds and to decrease the heating rate beneath the clouds. The increased heating within the cloud arises primarily from the greater photon path due to multiple scattering and in part from the 100% relative humidity. As shown in Fig. 15, most of the heating within clouds occurs near the top of the cloud where the downward and upward fluxes are largest. The decreased heating in the lower layers is a consequence of the reduced solar flux beneath the cloud. There is also a somewhat increased heating above the clouds due to absorption of reflected radiation.

Absorption by cloud drops was not included in the computations for Figs. 14 and 15. We estimated the error due to this omission by computing the absorption due to cloud droplets for a cloud of optical thickness $\tau^c=8$ with no water vapor included. The single scattering albedo for water droplets was computed from Mie
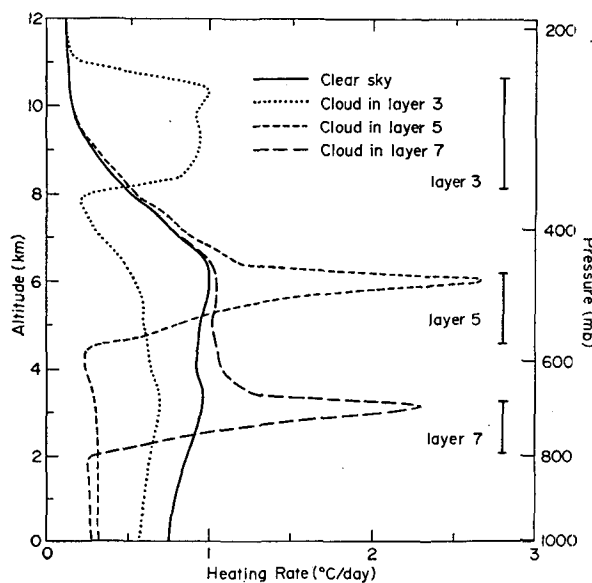

FIG. 15. Heating rates in the troposphere computed for water vapor absorption. The results are computed with the parameterization described in the text, but the doubling and adding methods are used and the atmosphere is divided into 45 layers. The standard atmosphere and water vapor distribution of McClatchey et al. (1972) is used, except that the relative humidity is 100% in the layer containing a cloud. The solar zenith angle is $\theta_0=60°$ and the ground albedo $R_g=0.07$.

theory at all wavelengths $\leqslant 4\ \mu m$ for which Irvine and Pollack (1968) tabulate the optical constants of water. The particle size distribution used was that given by Eq. (1) of Hansen (1971b) with a mean effective radius $a=10\ \mu m$ and an effective variance $b=0.2$. The absorption by the cloud droplets, integrated over wavelength and zenith angle, was found to be $\sim 5\%$ of the total solar flux.

The same amount of absorption, 5%, would occur if the cloud particles were non-absorbing and the cloud contained 0.08 cm of water vapor. Since absorption by liquid water takes place in roughly the same spectral interval as for the gas, it is perhaps a good approximation to include the effect of the cloud drops as an effective water vapor amount in computing $\bar{\omega}_{l,n}$. For a cloud containing 0.20 cm of water vapor, typical of middle level clouds, the addition of 0.08 cm increases the total absorption in the cloud from 7% to 7.7%. The relative effect of cloud particle absorption would be greater for cirrus clouds, which have larger particles and less water vapor. However, we have not completed the parameterization of cloud particle absorption as a function of cloud type, nor have we tested the error in such an approximation.

5. Surface absorption

Solar radiation transmitted by the atmosphere is subject to possible absorption at the earth's surface. The amount of absorption by the surface is large, approximately twice the total absorption in the atmosphere (Sasamori et al., 1972). The parameterization of the surface absorption is straightforward, following almost immediately once the transmission of the atmosphere has been obtained.

We divide the surface absorption into two parts, one $(A_{g,1})$ for those wavelength regions where the absorption coefficient of water is significant and one $(A_{g,2})$ for the remaining wavelengths. Approximately 35% of the solar flux is contained in the regions of significant water vapor absorption, as indicated by the probability distribution (Table 1); the same percentage is obtained from the assumption that water vapor absorption is significant only for wavelengths $>0.9\ \mu m$ (Joseph, 1971).

a. Clear skies

For clear skies, in the spectral regions associated with significant water vapor absorption, the fraction of the total solar flux absorbed at the ground is given by

$$A_{g,1}=\mu_0[0.353-A_{wv}(Mw_t)](1-R_g), \qquad (39)$$

where w_t is the effective water vapor amount in a vertical column above the ground.

For the spectral regions of negligible water vapor absorption the effect of Rayleigh scattering is included along with a correction for ozone absorption. In this clear sky case the fraction of the total solar flux absorbed by the ground is

$$A_{g,2}=\mu_0[0.647-\bar{R}_r(\mu_0)$$
$$-A_{oz}(Mu_t)](1-R_g)/(1-\bar{R}_r^*R_g), \quad (40)$$

where u_t is the ozone amount in a vertical path above the ground, $\bar{R}_r(\mu_0)$ the atmospheric albedo due to Rayleigh scattering, and $\bar{R}_r^*$ is the spherical albedo of the Rayleigh atmosphere for illumination from below; $\bar{R}_r$ is given by[14]

$$\bar{R}_r(\mu_0)=\frac{0.28}{1+6.43\mu_0}, \qquad (41)$$

which is a least-square fit (accurate to within $\sim 1\%$) to the results of numerical computations with the doubling and adding method; the computations for Rayleigh scattering were made with the U. S. Standard Atmosphere (Champion et al., 1962), using the molecular scattering coefficients given by Penndorf (1957) and the ozone distribution (17) with $a=0.4$ cm, $b=20$ km and $c=5$ km. (We used 17 Gauss points and 21 layers, with ~ 200 wavelengths for the spectral integration; the results were practically identical to those obtained for 60 layers in Section 2.) The numerical value for $\bar{R}_r^*=0.0685$ which is larger than $\bar{R}_r$. This is a result of the fact that most of the ozone absorption occurs near the top of the atmosphere.

b. Cloudy skies

For cloudy skies $A_{g,1}$ is obtained by multiplying the total transmission at the ground for each value of k_n by the factor $(1-R_g)p(k_n)$ and summing over the values of n for the region of significant water vapor absorption ($n=2-8$ for the discrete distribution of absorption coefficients in Table 1).

In computing $A_{g,2}$ for cloudy skies we neglect Rayleigh scattering. Thus, the fraction of the solar constant absorbed at the ground is

$$A_{g,2}=\mu_0[0.647-A_{oz}(Mu_t)]$$
$$\times[1-\bar{R}_a(\mu_0)](1-R_g)/(1-\bar{R}_a^*R_g), \quad (42)$$

where u_t is the ozone amount in a vertical path above the highest cloud layer, and $\bar{R}_a(\mu_0)$ and $\bar{R}_a^*$ refer to the visual cloud albedo given by (19).

----

[14] The average of $\bar{R}_r(\mu_0)$ over all sun angles is 6.0% for the entire solar spectrum. This albedo depends on the solar flux distribution and to a lesser extent on the ozone amount. With the solar flux of Labs and Neckel (1968) replaced by that of Johnson (1954) the albedo becomes 6.46%. For the more recent solar flux of Thekaekara (1973) the spherical albedo for Rayleigh scattering is 6.22%. Computations with ozone amounts of 0.25 and 0.50 cm (with the solar flux of Labs and Neckel) yield albedos of 6.15% and 5.93%, respectively, and show that (41) is nearly independent of ozone amount. Coulson (1959) obtained a Rayleigh albedo for the earth of 6.9%, apparently due to an underestimate of ozone absorption.

6. Discussion

The parameterizations derived for the absorption of solar radiation by ozone, water vapor and the earth's surface are being used in current versions of the GISS model of the global atmosphere (Somerville et al., 1974a). The computation time required for these parameterizations is small; the total time used by the numerical circulation model is increased by only ~0.3% as compared to the case of no solar radiation calculations.

With these parameterizations the concentrations and distributions of the major absorbers and scatterers of solar radiation are permitted to be variables. This is useful for investigating the effects of possible changes in the atmospheric composition, including "feedbacks" through the atmospheric dynamics. With this treatment of solar radiation the GISS numerical circulation model is being used to study the possible effects of changes in the solar energy spectrum and changes in the stratospheric ozone distribution (Somerville et al., 1974b).

The impact of solar radiation on weather forecasting has yet to be fully assessed. Rodgers (1972) argues that systematic errors in the radiation $\gtrsim 0.2$C day^{-1} will significantly degrade the quality of a two-week forecast. This suggests that for such an application it is worthwhile to aim at keeping systematic errors in the radiation from exceeding the order of 10%. In any case, the task of establishing the impact of solar radiation on the atmospheric motions provides one reason for developing reliable methods for computing that energy input.

The parameterization for ozone absorption has a high accuracy, exceeding the accuracy with which the ozone concentration is likely to be known in most applications. There is thus little incentive to seek a more accurate approach.

In the case of water vapor absorption we do not have satisfactory checks on the accuracy of the parameterization. Inaccuracies arise from errors in the laboratory transmission functions, from the scaling approximation, from the use of a single k-distribution for the entire spectrum, from the two-stream approximation for cloud albedos, and from the neglect of absorption by cloud drops. The absorption by cloud drops could probably be accounted for in terms of an effective water vapor amount as mentioned in the text. The simple two-stream equation for cloud albedos could be replaced by equations accounting for the zenith angle dependence or by any other rapid method for multiple-scattering computations. It would also be possible to use a number of k-distributions, say for each of the significant absorption bands; the scaling could then be different for each band. However, the usefulness of such modifications depends on the accuracy and completeness of laboratory data.

A test of the parameterization for water vapor could be made with realistic model spectral absorption coefficients, monochromatic multiple scattering computations, and integrations over wavelength. It would also be interesting to have comparisons of the parameterization to measurements of the solar flux in the atmosphere. But even with accurate observations it may be difficult to assign any discrepancies with the theory to particular approximations in the parameterization or to other causes. On the other hand, it will be possible to obtain an important check on the reliability of the computations by means of satellite measurements of the local albedo simultaneously with measurements of the cloud cover and cloud type. Such measurements do not directly yield the vertical distribution of absorbed solar energy, but for different local conditions (e.g., of cloud cover, sun angle, surface condition) the absorption is concentrated in different parts of the atmosphere. Thus, by comparison with many such measurements it will be feasible to obtain a diagnostic analysis of the methods of computation. Present satellite measurements of the global albedo have been used for a very crude check: the global albedo of ~29% measured by Raschke et al. (1973) is in satisfactory agreement with the value of ~31% obtained in the GISS model with 50% cloud cover (Somerville et al., 1974a).

We have not included here parameterizations for absorption by O_2 and CO_2. These are minor absorbers compared to O_3 and H_2O, but their contribution is significant for some applications. According to Sasamori et al. (1972) O_2 and CO_2 together are responsible for ~8% of the absorption in the atmosphere, corresponding to ~$2\frac{1}{2}$% of the absorption by the atmosphere plus surface. O_2 absorption is easy to handle since most of it occurs in a narrow region free of other gaseous absorption (cf. Fig. 1 and Houghton, 1963). CO_2 absorption overlaps H_2O and requires greater care (cf., Houghton, 1963; Howard et al., 1956). Formulas for absorption by O_2 and CO_2 are also given by Sasamori et al. (1972). The effect of scattering is not important for either O_2 or CO_2, except in the case of cloudy skies.

We have also excluded the effect of aerosols on absorption. Although aerosols also belong in the class of minor absorbers, their effect is variable and not well known; quite a number of computations of aerosol absorption have been initiated in the last few years (e.g., Yamamoto and Tanaka, 1972; Braslau and Dave, 1973). A reliable parameterization of aerosol absorption is needed, but will require a major study in itself.

REFERENCES

Arking, A., and K. Grossman, 1972: The influence of line shape and band structure on temperatures in planetary atmospheres. *J. Atmos. Sci.*, **29,** 937–949.

Braslau, N., and J. V. Dave, 1973: Effect of aerosols on the transfer of solar energy through realistic model atmospheres, Parts I & II. *J. Appl. Meteor.*, **12**, 601–619.

Champion, D. W. O'Sullivan and S. Telewes, Eds., 1962: *United States Standard Atmosphere.* Washington, D. C., Gov't. Printing Office, 278 pp.

Chandrasekhar, S., 1960: *Radiative Transfer.* New York, Dover, 393 pp.

Coulson, K. L., 1959: Characteristics of the radiation emerging from the top of a Rayleigh atmosphere—II Total upward flux and albedo. *Planetary Space Sci.*, **1**, 277–284.

Craig, R. A., 1951: Radiative temperature changes in the ozone layer. *Compendium of Meteorology*, Boston, Amer. Meteor. Soc., 292–302.

Dave, J. V., and P. M. Furukawa, 1967: The effects of scattering and ground reflection on the solar energy absorbed by ozone in a Rayleigh atmosphere. *J. Atmos. Sci.*, **24**, 175–181.

Fowle, F. E., 1915: The transparency of aqueous vapor. *Astrophys. J.*, **42**, 394–411.

Goody, R. M., 1964: *Atmospheric Radiation.* London, Oxford University Press, 436 pp.

Green, A. E. S., 1964: Attenuation by ozone and the earth's albedo in the middle ultraviolet. *Appl. Opt.*, **3**, 203–208.

Hansen, J. E., 1971a: Multiple scattering of polarized light in planetary atmospheres. Part I. The doubling method. *J. Atmos. Sci.*, **28**, 120–125.

——, 1971b: Multiple scattering of polarized light in planetary atmospheres. Part II. Sunlight reflected by terrestrial water clouds. *J. Atmos. Sci.*, **28**, 1400–1426.

——, and J. B. Pollack, 1970: Near-infrared light scattering by terrestrial clouds. *J. Atmos. Sci.*, **27**, 265–281.

Hering, W. S., C. N. Touart and T. R. Borden, 1967: Ozone heating and radiative equilibrium in the lower stratosphere. *J. Atmos. Sci.*, **24**, 402–413.

Herman, B. M., and D. N. Yarger, 1966: Some effects of multiple scattering on heating rates in the ozone layer. *J. Atmos. Sci.*, **23**, 320–324.

Houghton, J. T., 1963: The absorption of solar infra-red radiation by the lower stratosphere. *Quart. J. Roy. Meteor. Soc.*, **89**, 319–331.

Hovenier, J. W., 1969: Symmetry relationships for scattering of polarized light in a slab of randomly oriented particles. *J. Atmos. Sci.*, **26**, 488–499.

——, 1971: Multiple scattering of polarized light in planetary atmospheres. *Astron. Astrophys.*, **13**, 7–29.

Howard, J. N., D. E. Burch and D. Williams, 1956: Infrared transmission of synthetic atmospheres, Parts I–V. *J. Opt. Soc. Amer.*, **46**, 186–190, 237–241, 242–245, 334–338, 452–455.

——, J. I. F. King and P. R. Gast, 1961: Thermal radiation. *Handbook of Geophysics*, New York, Macmillan, Chap. 16.

Inn, E. C. Y., and Y. Tanaka, 1953: Absorption coefficient of ozone in the ultraviolet and visible regions. *J. Opt. Soc. Amer.*, **43**, 870–873.

Irvine, W. M., and J. B. Pollack, 1968: Infrared optical properties of water and ice spheres. *Icarus*, **8**, 324–360.

Johnson, F. S., 1954: The solar constant. *J. Meteor.*, **11**, 431–439.

Joseph, J. H., 1971: On the calculation of solar radiation fluxes in the troposphere. *Solar Energy*, **13**, 251–261.

Kondratyev, K. Ya., 1969: *Radiation in the Atmosphere.* New York, Academic Press, 912 pp.

Korb, G., J. Michalowsky and F. Möller, 1956: Investigations of the heat balance of the troposphere. AFCRL TN-56-881, 94 pp.

Labs, D., and H. Neckel, 1968: The radiation of the solar photosphere from 2000 Å to 100 μ. *Z. Astrophys.*, **69**, 1–73.

Manabe, S., and F. Möller, 1961: On the radiative equilibrium and heat balance of the atmosphere. *Mon. Wea. Rev.*, **89**, 503–532.

——, and R. F. Strickler, 1964: Thermal equilibrium of the atmosphere with a convective adjustment. *J. Atmos. Sci.*, **21**, 361–385.

McClatchey, R. A., R. W. Fenn, J. E. A. Selby, F. E. Volz and J. S. Garing, 1972: Optical properties of the atmosphere (3rd ed.). AFCRL Envirn. Res. Papers No. 411, 108 pp.

Napier, W. McD., 1970: A method for the construction of model stellar atmosphere. *Mon. Not. Roy. Astron. Soc.*, **147**, 287–293.

Paltrige, G. W., 1973: Direct measurement of water vapor absorption of solar radiation in the free atmosphere. *J. Atmos. Sci.*, **30**, 156–160.

Peebles, G. H., and M. S. Plesset, 1951: Transmission of gamma rays through large thicknesses of heavy materials. *Phys. Rev.*, **81**, 430–439.

Penndorf, R., 1957: Tables of the refractive index for standard air and the Rayleigh scattering coefficient for the spectral region between 0.2 and 20.0 μ and their application to atmospheric optics. *J. Opt. Soc. Amer.*, **47**, 176–182.

Pettit, E., 1951: *The Sun and Stellar Radiation in Astrophysics*, J. Hynek, Ed. New York, McGraw-Hill, 703 pp.

Prabhakara, C., B. J. Conrath, L. J. Allison and J. Steranka, 1971: Seasonal and geographic variation of atmospheric ozone, derived from Nimbus 3. NASA TN D-6443, 61 pp.

Raschke, E., T. H. Vonder Harr, W. R. Bandeen and M. Pasternak, 1973: The annual radiation balance of the earth-atmosphere system during 1969–70 from Nimbus 3 measurements. *J. Atmos. Sci.*, **30**, 341–364.

Redheffer, R., 1962: On the relation of transmission-line theory to scattering and transfer. *J. Math. Phys.*, **41**, 1–41.

Rodgers, C. D., 1967: The radiative heat budget of the troposphere and lower stratosphere. Rept. No. A2, Planetary Circulations Project, Dept. of Meteorology, M.I.T., 99 pp.

——, 1972: Parameterization of sub-grid scale processes. GARP Publication Series, W.M.O., No. 8, 6–19.

Sagan, C., and J. B. Pollack, 1967: Anisotropic nonconservative scattering and the clouds of Venus. *J. Geophys. Res.*, **72**, 469–477.

Sasamori, T., J. London and D. V. Hoyt, 1972: Radiation budget of the Southern Hemisphere. *Meteor. Monogr.*, **13**, No. 35, 9–23.

Somerville, R. C. J., P. H. Stone, M. Halem, J. E. Hansen, J. S. Hogan, L. M. Druyan, G. Russell, A. A. Lacis, W. J. Quirk and J. Tenenbaum, 1974a: The GISS model of the global atmosphere. *J. Atmos. Sci.*, **31**, 84–117.

——, J. E. Hansen, A. A. Lacis, W. J. Quirk and P. H. Stone, 1974b: Numerical experiments on short-term meteorological effects of solar variability. *Proc. Symp. Possible Relationships between Solar Activity and Meteorological Phenomena*, NASA GSFC Report (in press).

Thekaekara, M. P., 1973: Solar energy outside the earth's atmosphere. *Solar Energy*, **14**, 109–127.

van de Hulst, H. C., 1963: A new look at multiple scattering. Tech. Rept., Goddard Institute for Space Studies, NASA, New York, 81 pp.

Vigroux, E., 1953: Contributions a l'étude expérimentale de l'absorption de l'ozone. *Ann. Phys.*, **8**, 709–762.

Yamamoto, G., 1962: Direct absorption of solar radiation by atmospheric water vapor, carbon dioxide and molecular oxygen. *J. Atmos. Sci.*, **19**, 182–188.

——, and M. Tanaka, 1972: Increase of global albedo due to air pollution. *J. Atmos. Sci.*, **29**, 1405–1412.